Journal of The Korean Society for Geo-Spatial Information System
Vol.10 No.5/ Dec 2002/ pp.53-65

# Fusion of DEMs Generated from Optical and SAR Sensor

**Jin, Kyeong Hyeok* · Yeu, Yeon** · Hong, Jae Min*** · Yoon, Chang Rak**** · Yeu, Bock Mo*****

ABSTRACT

The most widespread techniques for DEM generation are stereoscopy for optical sensor images and SAR interferometry(InSAR) for SAR images. These techniques suffer from certain sensor and processing limitations, which can be overcome by the synergetic use of both sensors and DEMs respectively. This study is associated with improvements of accuracy with consistency of image's characteristics between two different DEMs coming from stereoscopy for the optical images and interferometry for SAR images. The MWD(Multiresolution Wavelet Decomposition) and HPF(High-Pass Filtering), which take advantage of the complementary properties of SAR and stereo optical DEMs, will be applied for the fusion process. DEM fusion is tested with two sets of SPOT and ERS-1/-2 satellite imagery and for the analysis of results, DEM generated from digital topographic map(1 to 5000) is used. As a result of an integration of DEMs, it can more clearly portray topographic slopes and tilts when applying the strengths of DEM of SAR image to DEM of an optical satellite image and in the case of HPF, the resulting DEMs are improved in terms of RMSE for a reference DEM.

***Key words*** : DEM fusion, stereoscopy, SAR interferometry, multiresolution wavelet decomposition, high-pass filtering

## 1. Introduction

DEM is a digital cartographic representation of elevation for the terrain at regularly spaced intervals in x and y directions, using z-values referenced to a common vertical datum. It is used in the ortho-correction of aerial or satellite images, the generation of contour map, the hydrologic modeling of flood hazards, terrain analysis (hillshade, slope, aspect...) and is applied in GSIS as based map data. The two major techniques for DEM generation from satellite imagery are stereoscopy for the

* Researcher of Sokkok Institute of Observational Science & Technology, 02)3453-9800, tom51@sog.or.kr
** Graduate student at the University of Wisconsin-Madison, yeu@cae.wisc.edu
*** Researcher of Sokkok Institute of Observational Science & Technology, 02)3453-9800, alssmile@sog.or.kr
**** Researcher of Computer & Software Technology Laboratory/ETRI, 042)860-5833, cryoon@etri.re.kr
***** President of Sokkok Institute of Observational Science & Technology, 02)3453-9800, yeubm@sog.or.kr

optical images and interferometry for SAR images. Both techniques extract the elevation information using different methods and each of them has different characteristics.

The technique of stereoscopy for optical satellite images obtains the elevation information through image matching on the overlapping area of two images. In case of SPOT panchromatic images, vertical accuracy is defined as a root mean square error of about 15-20m. But when acquiring stereo images, cloud cover is a consistent problem that prevents the use of optical satellite images in wide areas. If we take image pair acquired from different-pass, it could bring the mismatching of conjugate points on overlapping images and spikes in resulting DEM.

The SAR interferometry determines the location of a point in three dimensions using the phase difference between two SAR images acquired from two repeated SAR coverages. In SAR interferometry, a key step to obtain the elevation information is the phase unwrapping which calculates the elevation of each pixel by adding the correct integer number of phase cycles to each phase measurement. Phase unwrapping can also be used to correct unavoidable height errors which are occasionally due to the SAR image acquisition geometry and surface cover. Because SAR which is an active remote sensor(sends out its own pulse of radio waves, receives the scattered pulses, measures the energy that is reflected or scattered back from the target material), in contrast to the optical satellite system, it produce all weather, day and night, high resolution images of the terrain surface.

These techniques suffer from certain sensor and processing limitations, which can be overcome by the synergetic use of both sensors and DEMs respectively. The goal of DEM fusion is to create new DEMs that fully represents the terrain surface and the accuracy for the reference DEM is improved by integrating two DEMs of the InSAR DEM and the stereo optical DEM. In this study, we apply discrete two-dimensional wavelet transform and the filtering technique to combine DEMs generated from optical satellite images and SAR images.

## 2. Characteristics of InSAR and stereo optical DEM

For the stereo optical DEM, it happens often that there are gaps and empty spaces between the observed points, or that the point distribution is generally poor because image matching process is performed leaving a consistent space. In such cases, different interpolation methods can give quite different results and resulting DEMs are not detailed. When image matching process is performed densely to determine conjugate point on overall overlapping area of stereo images, it is not easy to acquire corresponding image points and partially spikes with large error induced by mismatching. Also, if using stereo images with multitemporal or radiometric difference, errors occur locally in image matching process.

In contrast to the stereo optical DEM, the InSAR DEM represents in detail the continuous variation of relief over the terrain surface. Problems occur where the terrain leads to effects like layover or shadowing, causing corrupted or no return signals. Beside terrain-induced problems, the repeat pass image acquisition contributes to the error. Typically, the ERS satellite have a 35-day repeat cycle, during which changes in the backscatter geometry of the ground resolution elements may occur and cause a decorrelation of the signals.

## 3. DEM fusion

### 3.1 Multiresolution Wavelet Decomposition (MWD)

As a concept of decomposing two-dimensional signals into multiresolutioin representation, a multiresolution wavelet representation discriminates several orientation. Also, the multiresolution analysis based on wavelets theory provides a simple hierarchical framework for interpreting signals.

Figure 1 is a convenient description of multiresolution analysis and more generally of pyramid algorithms(Mallat, 1989). The base of the pyramid is the original data(ex. DEM). Each level of the pyramid is an approximation of the original DEM computed from the original one. When climbing the pyramid, the successive approximations have coarser and coarser spatial resolutions. The computation of the approximations is done using a base of

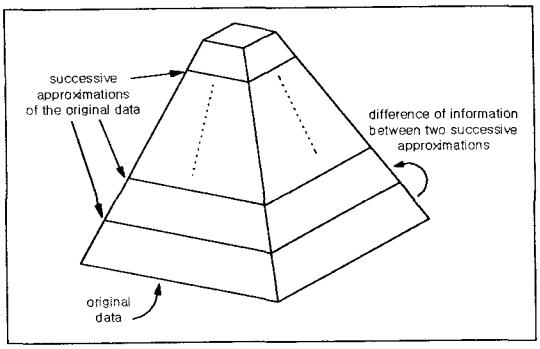


**Figure 1. Pyramid structure of multiresolutoin wavelet analysis**

functions, called the scale functions. In this scheme, the use of the wavelet transform allows the description of the differences existing between two successive approximations of the same DEM. If the process of multiresolution analysis is inverted, the original DEM can be exactly reconstructed from one approximation and the different wavelet coefficients describing the differences in DEM between this approximation and the original DEM.

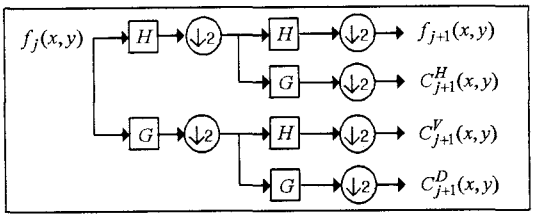


**Figure 2. Multiresolution analysis structure**

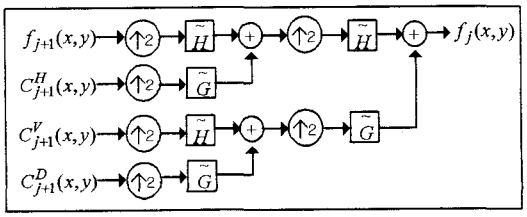


**Figure 3. Multiresolution synthesis structure**

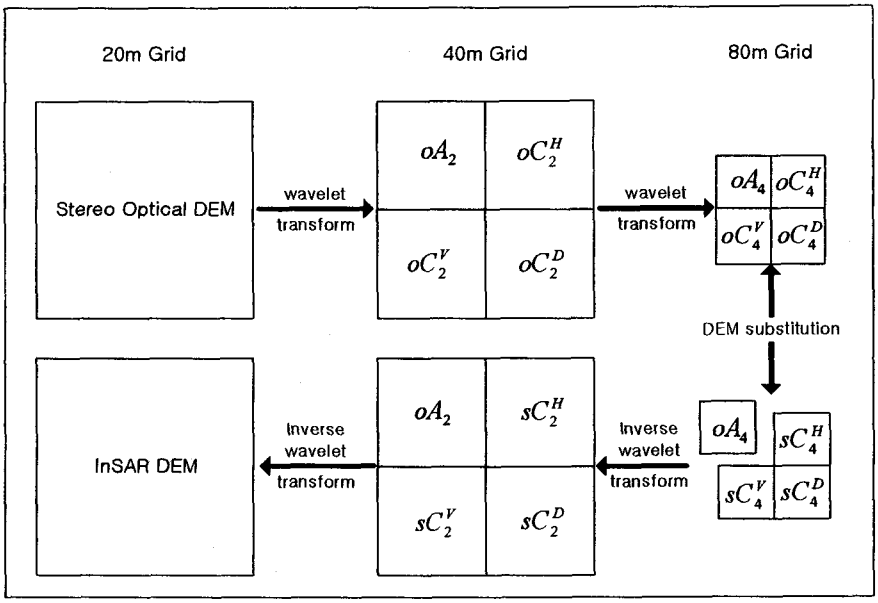


**Figure 4. General scheme for DEM fusion using MWD**

Mallat's algorithm can be implemented using a filter bank structure(Figure 2 and Figure 3). $f_j(x, y)$ represents the original signal, where x is the column, and y is the line or row. The columns and rows are processed separately. Filter $H$ is applied to the column of $f_j(x, y)$, and the same is done for filter $G$. Then on each resulting DEMs filter $H$ and $G$ is applied. Resulting DEMs are four DEMs of $f_{j+1}(x, y)$, $C^H_{j+1}(x, y)$, $C^V_{j+1}(x, y)$, $C^D_{j+1}(x, y)$.

## 3.2 MWD method for DEM fusion

DEM fusion using MWD is similar to image fusion that combines both high spatial and high spectral resolution images with the aim of obtaining the most complete and accurate description of the observed area. To begin with, after creating the raster files of the InSAR DEM and the stereo optical DEM in which each grid cell value contains an elevation value, MWD is applied to both DEMs. DEM fusion is performed through the inverse wavelet transform using the three wavelet coefficients DEMs[ $C^H_{j+1}(x, y)$, $C^D_{j+1}(x, y)$ $C^V_{j+1}(x, y)$,] of the InSAR DEM and the approximation[ $f_{j+1}(x, y)$] of the stereo optical DEM. Therefore, the InSAR DEM includes the differences between elevation informations of adjacent grid cell. The accuracy of the stereo optical DEM for the reference DEM is better than that of the InSAR DEM. So, as preserving the accuracy of stereo optical DEM and complementing the information of the InSAR DEM, new DEM with the properties of the stereo optical DEM and the InSAR DEM is generated. Figure. 4 illustrates the process of integrating the InSAR DEM and the stereo optical DEM with 20m spatial

resolution.

Table. 1 and 2 are the four-tap filters designed by Daubechies(1988). In this study, we integrate the InSAR DEM and the stereo optical DEM applying the decomposition level(DL) of 1, 2, 3, 4, 5.

**Table 1. Value of the coefficients of the filter for the decomposition of wavelet transform**

| n | $H$ filter | $G$ filter |
|---|---|---|
| 0 | -0.129409522551 | -0.482962913145 |
| 1 | 0.224143868042 | 0.836516303738 |
| 2 | 0.836516303738 | -0.224143868042 |
| 3 | 0.482962913145 | -0.129409522551 |

**Table 2. Value of the coefficients of the filter for the synthesis of wavelet transform**

| n | $\bar{H}$ filter | $\bar{G}$ filter |
|---|---|---|
| 0 | 0.482962913145 | -0.129409522551 |
| 1 | 0.836516303738 | -0.224143868042 |
| 2 | 0.224143868042 | 0.836516303738 |
| 3 | -0.129409522551 | -0.482962913145 |

### 3.3. HPF method for DEM fusion

In applications of digital image processing, filtering techniques are used to extract a high frequency and a low frequency content from images. Generally, applying low-pass filter to images, noise is removed and has the effect of blurring the image. And high-pass filtering is a linear filtering operation and is the opposite of low-pass filtering. As it can be easily guessed it is used to emphasize the high frequency content of the image. This has similar concepts of MWD. HPF used in this study is a variation of previously researched techniques and consists of three basic steps:(1) perform a low-pass filter on the stereo optical DEM to extract the low frequency information preserving the accuracy of it for the reference DEM, (2) perform a high-pass filter on the InSAR DEM to extract the differences between adjacent grid cell of that, (3) calculate the sum of the high-pass and low-pass filtered results to create a fused DEM(Figure. 5).

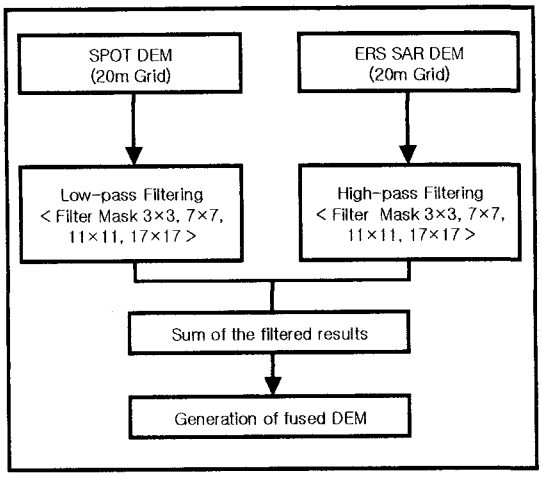


**Figure 5. Flow of DEM fusion using HPF**

It is important to select the size of filter kernel being applied to the InSAR DEM and the stereo optical DEM. So, we used the various filter kernels of 3×3, 7×7, 11×11, 17×17 and compared with resulting fused DEMs.

## 4. DEM generation and results analysis

### 4.1 Test data and DEM generation

The stereo optical DEM was derived from a SPOT panchromatic image pair using ERDAS IMAGINE 8.5 S/W and the InSAR

DEM was generated from ERS-1/-2 SLC stereo images using EvInSAR 2.1 S/W. SPOT images were acquired on 15 November 1997, 2 November 1999 and ERS-1 SLC image was acquired on 22 January 1996, ERS-2 SLC image was acquired on 23 January 1996. And the computation system for DEM fusion is constructed on Visual C++ 6.0 program language. For results analysis, the reference DEM is generated from digital topographic map(1 to 5000) and all DEMs have the spatial resolution of 20m grid.

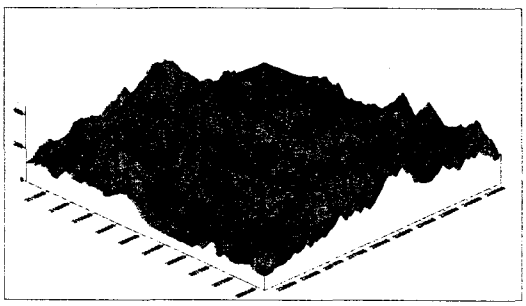

Figure 6. Reference DEM(study area Ⅰ)

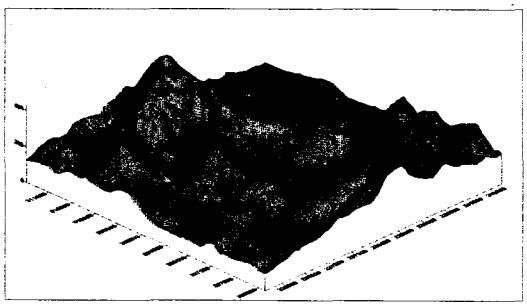

Figure 7. SPOT DEM(study area Ⅰ)

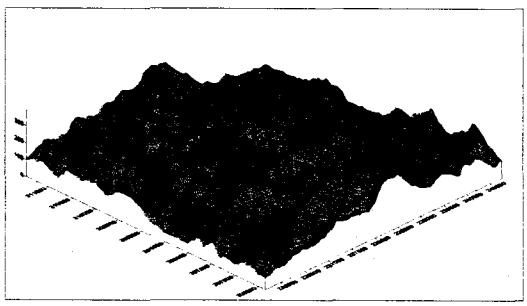

Figure 8. ERS SAR DEM(study area Ⅰ)

Figure 6 illustrates the three dimensional representation of the reference DEM for study area Ⅰ. Figure 7 and 8 show each the SPOT DEM and the ERS SAR DEM for study area Ⅰ. In Figure 7, the SPOT DEM represents roughly the terrain surface but the ERS SAR DEM of Figure 8 represents in detail the terrain and close to the reference DEM of Figure 6 but some spikes originated from geometric distortion of SAR images existed.

Figure 9, 10, and 11 are the resulting DEMs that integrate the ERS SAR DEM and the SPOT DEM when each decomposition level for MWD fusion method is 2, 3, and 4. As a result of an integration of two DEMs, it can more clearly portray topographic slopes and tilts when applying strengths of the ERS SAR DEM to the SPOT DEM. In the case of MWD fusion

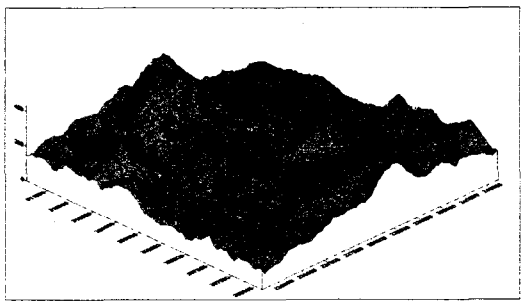

Figure 9. Fused DEM (MWD, DL=2, area Ⅰ)

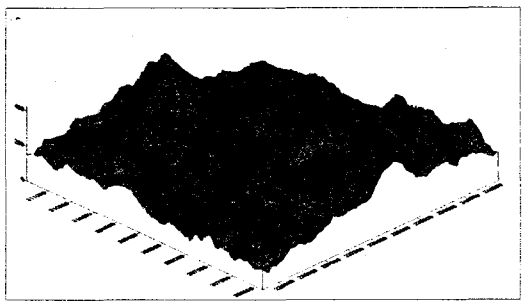

Figure 10. Fused DEM (MWD, DL=3, area Ⅰ)

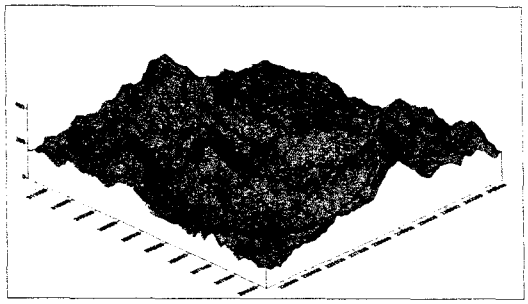

**Figure 11 Fused DEM (MWD, DL=5, area I )**

level in MWD method, it shows more characteristics of the ERS SAR DEM.

Figure 12, 13 and 14 are the fused DEMs using HPF fusion method, which each filter kernel is 7×7, 11×11, 17×17 kernel. Like the results of MWD fusion method, as the size of filter kernel increases, the resulting DEMs represent more in detail the terrain surface than the SPOT DEM and is close to the reference DEM by locally complementing the elevation information of the SPOT DEM's grids that have a large error for the reference DEM.

## 4.2 Analysis of Results

In the analysis of results, we used the statistics of the mean, standard deviation, root mean square error(RMSE) for the reference DEM to assess the quality of a fused DEM for fusion methods and a cross sectional view of each DEM. And the semivariogram that is a plot of semivariance against lag, reflects the underlying structure of spatial variability is used.

### 4.2.1 Comparison of the Statistics

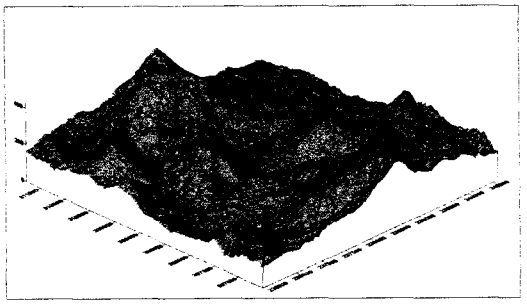

**Figure 12. Fused DEM (HPF, 7×7, study area I )**

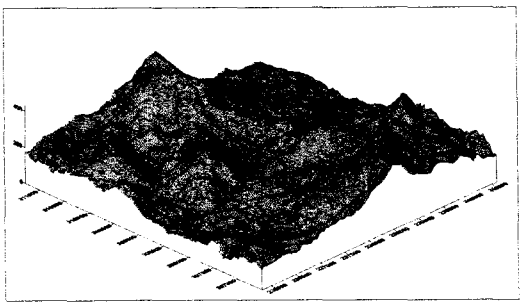

**Figure 13. Fused DEM (HPF, 11×11, study area I )**

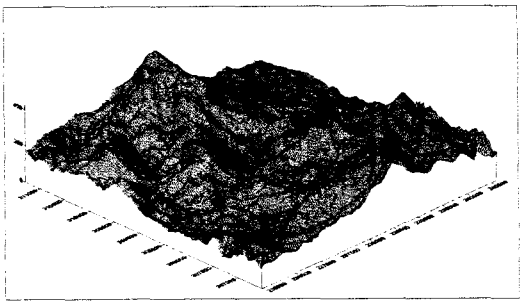

**Figure 14. Fused DEM (HPF, 17×17, study area I )**

The results of the fusion procedure are listed in Table 3, 4, where also the errors before fusion, with which achieved the best results, are given. Table 3 shows the statistics of the SPOT DEM, the ERS SAR DEM and the resulting DEMs for MWD fusion method. When comparing the statistics of the SPOT DEM with the reference DEM, the differences between

**Table 3. Statistics of the results from MWD fusion**

| Study area | DEM | Mean | Standard deviation | RMSE |
|---|---|---|---|---|
| I | Reference DEM | 186.180 | 72.936 | - |
| | SPOT DEM | 189.276 | 72.028 | 16.197 |
| | ERS SAR DEM | 145.225 | 75.401 | 48.178 |
| | MWD(DL1) | 189.276 | 72.057 | 16.342 |
| | MWD(DL2) | 189.276 | 72.128 | 16.663 |
| | MWD(DL3) | 189.276 | 72.300 | 17.162 |
| | MWD(DL4) | 189.276 | 72.723 | 17.638 |
| | MWD(DL5) | 189.276 | 73.718 | 17.935 |
| II | Reference DEM | 200.592 | 90.369 | |
| | SPOT DEM | 197.292 | 90.846 | 28.885 |
| | ERS SAR DEM | 76.790 | 86.672 | 128.272 |
| | MWD DEM(DL1) | 197.292 | 90.794 | 28.986 |
| | MWD DEM(DL2) | 197.292 | 90.718 | 29.184 |
| | MWD DEM(DL3) | 197.292 | 90.598 | 29.505 |
| | MWD DEM(DL4) | 197.292 | 90.523 | 29.842 |
| | MWD DEM(DL5) | 197.292 | 89.907 | 30.754 |

**Table 4. Statistics of the results from HPF fusion**

| Study area | DEM | Mean | Standard deviation | RMSE |
|---|---|---|---|---|
| I | Reference DEM | 188.844 | 72.713 | - |
| | SPOT DEM | 191.968 | 71.914 | 16.286 |
| | ERS SAR DEM | 147.749 | 75.510 | 47.885 |
| | HPF DEM(3×3) | 191.968 | 71.927 | 16.234 |
| | HPF DEM(7×7) | 191.969 | 72.022 | 16.081 |
| | HPF DEM(11×11) | 191.971 | 72.191 | 15.892 |
| | HPF DEM(17×17) | 191.974 | 72.531 | 15.693 |
| II | Reference DEM | 201.862 | 87.757 | |
| | SPOT DEM | 198.319 | 88.219 | 29.571 |
| | ERS SAR DEM | 78.649 | 85.752 | 127.580 |
| | HPF DEM(3×3) | 198.320 | 88.213 | 29.490 |
| | HPF DEM(7×7) | 198.326 | 88.216 | 29.182 |
| | HPF DEM(11×11) | 198.333 | 88.265 | 28.778 |
| | HPF DEM(17×17) | 198.356 | 88.419 | 28.221 |

the mean, the standard deviation were low but in case of the ERS SAR DEM, the differences between the statistics for the reference DEM were high. As results of DEM fusion, the means and the standard deviations of fused DEMs were similar with those of SPOT DEM. For the study area I, the each standard deviation of fused DEMs is close to that of the reference DEM as compared with that of the SPOT DEM.

In the study area I, the RMSE of the SPOT DEM for the reference DEM is about 16m and that of the ERS SAR DEM is about 48m while in the study area II, each

of those is about 28m, 128m. As comparing the RMSE of fusion resulting DEMs with that of the initial SPOT DEM and ERS SAR DEM, in the case of MWD fusion technique, it increased after fusion by 1m in the study area I and by 6-10m in the study area II as compared with the RMSE of the SPOT DEM.

Table 4 presents the statistics of the SPOT DEM, ERS SAR DEM and DEMs integrated by HPF fusion technique. In contrast to the results of MWD fusion, as the size of filter kernels increased, the RMSE of the resulting DEMs of HPF decreased as compared with that of the SPOT DEM. For the results of the study area I, the RMSE of the fused DEMs decreased by 0.6m and for the results of the study area II, it decreased by 1.3m. As the results of the statistical analysis for HPF fusion technique, the resulting DEMs are improved in terms of RMSE.

4.2.2 Comparison of the Cross Sectional View

For the analysis of the characteristics for the representation of terrain surface, we compared with cross sections used for special applications to show a string of elevations along a designated line from point A to point B. Figure 15, for the study area I, shows the result of the cross section for the reference DEM, the SPOT DEM, the ERS SAR DEM, fused DEMs by MWD fusion technique with the decomposition level of 1, 2, 3. Figure 16 is the comparison of the cross sections for each DEM in the study area II. When

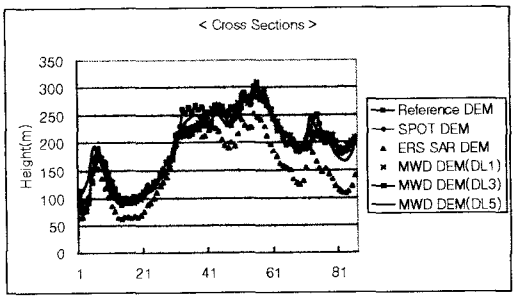


**Figure 15. Cross sections of DEMs (MWD, study area I)**

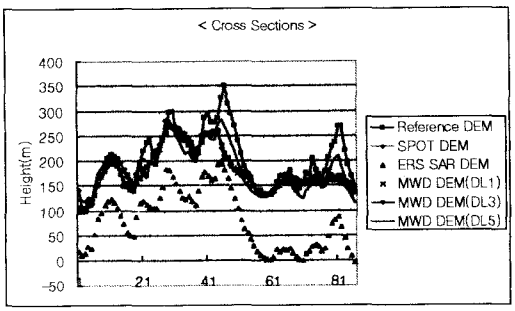


**Figure 16. Cross sections of DEMs (MWD, study area II)**

looking at the cross section of the ERS SAR DEM, the elevation informations are lower than the reference DEM all over. The cross section of the SPOT DEM is similar to that of the reference DEM but errors for areas with a steep slope locally existed.

As a result of the integration the SPOT DEM with the ERS SAR DEM, the fused DEMs have the characteristics of the ERS SAR that represent in detail the terrain surface complementing the errors of the SPOT DEM.

Figure 17, in the study area I, presents the result of the cross section for the reference DEM, the SPOT DEM, the ERS SAR DEM, the resulting DEMs of HPF method applying the 3×3, 7×7, 11×11, 17×17 filter kernel and Figure 16 shows

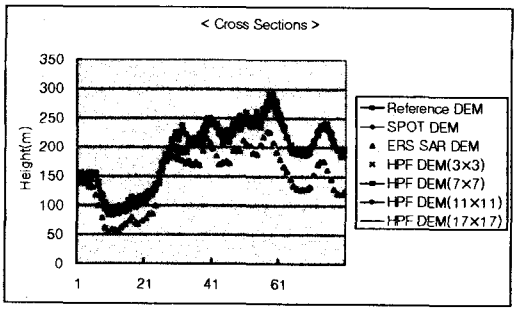


**Figure 17. Cross sections of DEMs (HPF, study area I )**

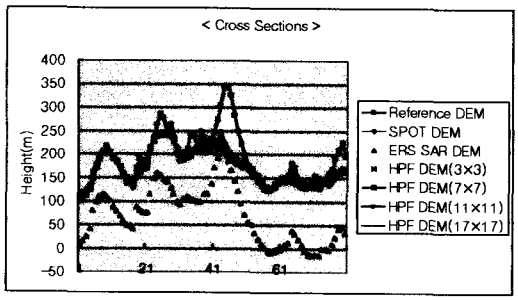


**Figure 18. Cross sections of DEMs (HPF, study area II)**

cross sections for the study area II. In the case of HPF fusion results, fused DEMs represent more fully the terrain surface as compared with the SPOT DEM but not as the results of MWD fusion technique.

As integrating the SPOT DEM with the ERS SAR DEM, it can give the detailed representation of DEM for the terrain surface and be close to the reference DEM. And areas which are not represented at the SPOT DEM can be complemented by the ERS SAR DEM

### 4.2.3 Comparison of Semivariogram

Semivariance is the primary tool of modern geostatistics, a field of analysis developed from regionalized variable theory for the modeling of continuous, non-deterministic surfaces exhibiting spatial dependence. Geostatistics were initially applied to mining geology, and were extended for analysis of the pattern and spatial structure of topographic surfaces (Brown et al, 1994).

Semivariance analysis describes a surface as the average squared difference of surface values which are a given distance, or lag, apart. Semivariance in a single dimension, $\gamma(h)$, is estimated by the expression.

$$\gamma(h) = \frac{1}{2(N-h)} \sum_{i=1}^{N-h} [z(i) - z(i+h)]^2 \quad (1)$$

where $N$ is the number of points on the surface, $z(i)$ is the value of the surface at any point $i$, and $z(i+h)$ is the value of the surface $h$ units from $i$. The shape of the semivariogram, a plot of semivariance against lag, is modeled using spherical, linear, or exponential equations. In this study, for analysis of fused DEMs, semivariograms for horizontal and vertical direction is applied.

Figure 19, in the study area I , shows the semivariograms of horizontal direction for the reulting DEMs using MWD fusion technique. Figure 20 presents the semivariograms of vertical direction. All semivariograms are similar to each other, especially the semivariograms of fused DEMs have not the remarkable differences for the initial SPOT DEM, the ERS SAR DEM and the reference DEM. The analysis of Figure 20 indicates the same as results of analysis of semivariograms for horizontal direction.

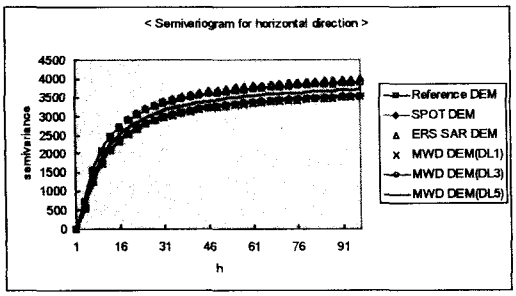


**Figure 19. Semivariograms of DEMs (MWD, horizontal, study area Ⅰ)**

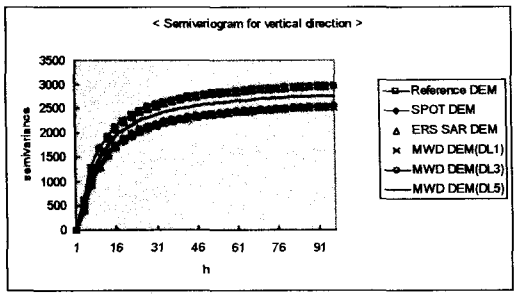


**Figure 20. Semivariograms of DEMs (MWD, vertical, study area Ⅰ)**

Figure 21 shows the semivariograms of horizontal direction for original DEMs and fused DEMs by HPF fusion method in the study area Ⅰ. All semivariograms are similar but each semivariogram of fused DEMs generated by HPF was close to that of the SPOT DEM.

Figure 22 through Figure 26 are the semivariograms of fused DEMs for the study area Ⅱ and most semivariograms have a similar shape but the semivariogram of the ERS SAR DEM was different from other semivariograms. And the semivariograms of fused DEMs are similar to the semivariogram of the SPOT DEM.

Figure 22 through Figure 26 are the semivariograms of fused DEMs for the study area Ⅱ and most semivariograms have a similar shape but the semivariogram of fused DEMs are similar to the semivariogram of the SPOT DEM.

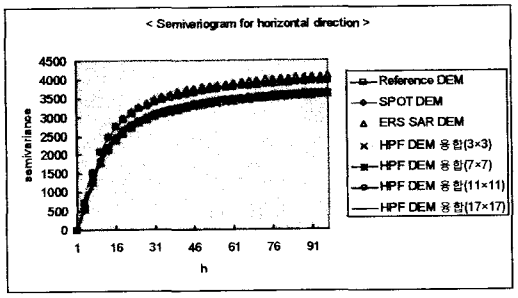


**Figure 21. Semivariograms of DEMs (HPF, horizontal, study area Ⅰ)**

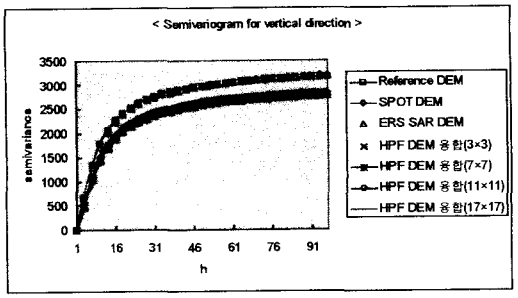


**Figure 22. Semivariograms of DEMs (HPF, vertical, study area Ⅰ)**

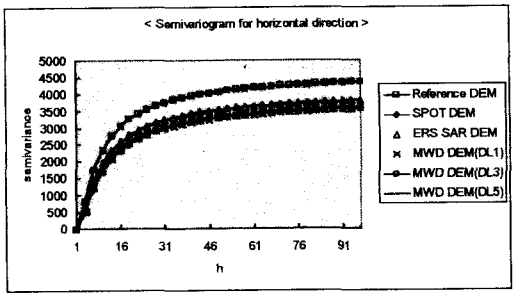


**Figure 23. Semivariograms of DEMs (MWD, horizontal, study area Ⅱ)**

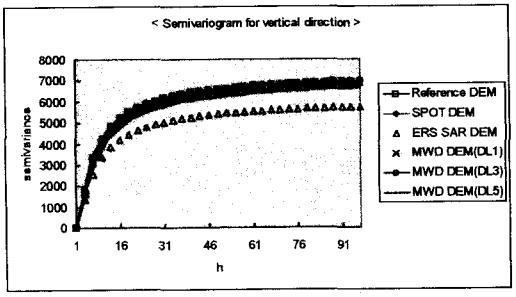


**Figure 24. Semivariograms of DEMs (MWD, vertical, study area Ⅱ)**

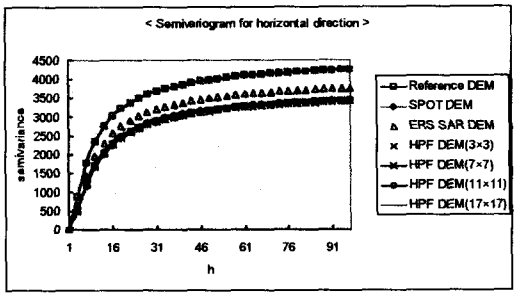


**Figure 25. Semivariograms of DEMs (HPF, horizontal, study area II)**

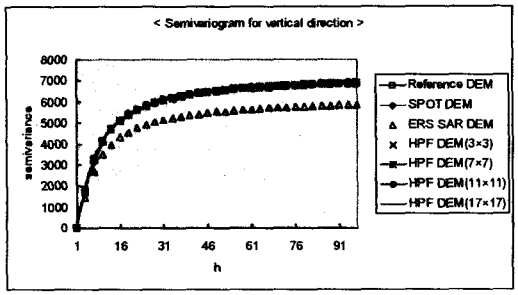


**Figure 26. Semivariograms of DEMs (HPF, vertical, study area II)**

Therefore, as the results of MWD and HPF fusion techniques, the characteristics of the SPOT DEM and the ERS SAR DEM are preserved and new DEMs that are close to the reference DEM, which represent more fully the terrain surface than the SPOT DEM and more accurate than the ERS SAR DEM, were generated.

## 5. Conclusions

We have presented the utility of DEM fusion such as MWD, HPF method applying to the SPOT DEM generated through stereoscopy and the ERS SAR DEM through SAR interferometry. As a result of fusion, it can be derived a fused DEM of higher quality in terms of accuracy and interpretability compared to that of a single source.

1. The SPOT DEM is more accurate than the ERS SAR DEM when analyzing the RMSE for the reference DEM. But the representation of SPOT DEM is rough, while the RMSE of the ERS SAR DEM is higher than that of the SPOT DEM but the ERS SAR DEM represents in detail the terrain.
2. As results of integration low frequency parts of the SPOT DEM with high frequency parts of the ERS SAR DEM, fused DEMs is close to the reference DEM while preserving the absolute accuracy of the SPOT DEM, as complementing each characteristic of the SPOT DEM and the ERS SAR DEM.
3. In the case of results of HPF fusion technique, as it increases the size of filter kernels, the RMSE for the reference DEM decreased, that the accuracy of fused DEMs improved. And those could not represent as fully as fused DEMs by MWD fusion technique.
4. We think that if fusing the stereo optical DEM with the InSAR DEM generated from SAR images with higher spatial resolution and optimal conditions for the extraction of DEM, higher quality DEMs would be generated and improved in terms of RMSE.

## Acknowledgements

This work was financially supported, in part, by Electronics and Telecommunications Research Institute.

## References


1. Al-Rousan, N., P. Cheng., G. Petrie., Th. Toutin, and M.J. Valadan Zoej., 1997. Automated DEM Extraction and Orthoimage Generation from SPOT Level 1B Imagery. *PE & RS*, Vol. 63, No. 8, pp. 965-974.
2. Blanc, P., Blu, T., Ranchin, T., Wald, L., and Aloisi, R., 1998. Using iterated filter banks with the ARSIS concept for producing 10m Landsat multispectral images. *International journal of Remote Sensing*. Vol.19, No.12, pp.2331-2343.
3. Bolstad, P. V., and Stowe, T., 1994. An Evaluation of DEM Accuracy: Elevation, Slope and Aspect, *PE & RS*, Vol.60, No.11, pp.1327-1332.
4. Brown, D. and Bara, T. (1994), Recognition and Reduction of Systematic Error in Elevation and Derivative Surfaces from 7.5-Minute DEMs, *PE & RS*, Vol. 60, No. 2, p. 189-194.
5. Daubechies, I., 1992. *Ten Lecture on Wavelets*. Society for Industrial and Applied Mathematics, Philadelphia, Pennsylvania. pp. 195-196.
6. Honikel, M., 1999. Strategies and methods for the fusion of digital elevation models from optical and SAR data. *IAPRS*, Vol. 32, Part 7-4-3 W6, Valladolid, Spain, pp. 83-89
7. Jeong, D.C., B.G. Kim., 2001. The Accuracy Assessment of DEMs Derived by SAR Interferometry. *Korean Society of Civil Engineers*, Vol.21, No.2-D, pp. 237-246.
8. Ka, M.H., M.J. Kim., 2001. Digital Elevation Model Generation using SAR Stereo Technique with Radarsat Images over Seoul Area. *Korean Journal of Remote Sensing*, Vol.17, No.2, pp.155-164.
9. Mallat. S.G, 1989. A Theory for Multiresolution Signal Decomposition: The Wavelet Representation. *IEEE Trans. Pattern Anal. Machine Intell*, Vol. 11. No. 7. pp. 674-693.
10. Ranchin, T., L. Wald, 2000. Fusion of High Spatial and Spectral Resolution Images: The ARSIS Concept and Its Implementation. *PE & RS*, Vol, 66. No, 1. pp. 49-61.
11. Seo, B.J., Y.I. Kim., Y.D. Eo., J.J. Jeong., 1998. A Comparison Study on the Techniques for DEM Extraction from SAR Imagery. *Korean Society for Geo-Spatial Information System*, Vol.6, No.2, pp. 21-34
12. Vrabel, J., 1996. Multispectral Imagery Band Sharpening Study. *PE & RS*, Vol.62, No.9, pp.1075-1083.
13. Yocky, D.A. 1996. Multiresolution Wavelet Decomposition Image Merger of Landsat Thematic Mapper and SPOT Panchromatic Data. *PE & RS*, Vol.62, No.9, pp.1067-1074.